Nanoscale

PAPER

View Article Online
View Journal | View Issue

Cite this: *Nanoscale*, 2019, **11**, 12177

Electromagnetic interactions of dye molecules surrounding a nanosphere†

Baptiste Auguié, *‡ Brendan L. Darby and Eric C. Le Ru ‡

Received 12th February 2019,
Accepted 22nd May 2019

DOI: 10.1039/c9nr01304k

rsc.li/nanoscale

Enhanced interaction between light and molecules adsorbed on metallic nanoparticles is a cornerstone of plasmonics and surface-enhanced spectroscopies. Recent experimental access to the electronic absorption spectrum of dye molecules on silver colloids at low molecular coverage has revealed subtle changes in the spectral shape that may be attributed to a combination of factors, from a chemical modification of the molecule in contact with a metal surface to electromagnetic dye–dye and dye–metal interactions. Here we develop an original model to rigorously address the electromagnetic effects. The dye molecules are described as coupled anisotropic polarisable dipoles and their interaction with the core metal particle is described using a generalised Mie theory. The theory is readily amenable to numerical implementation and yields far-field optical cross-sections that can be compared to experimental results. We apply this model to specific adsorption geometries of practical interest to highlight the effect of molecular orientation on predicted spectral shifts and enhancement factors, as a function of surface coverage. These are compared to experimental results and reproduce the measured spectral changes as a function of concentration. These results have direct implications for the interpretation of surface selection rules and enhancement factors in surface-enhanced spectroscopies, and of orientation and coverage effects in molecular/plasmonic resonance coupling experiments.

Metallic nanoparticles (NPs) such as gold or silver colloids can sustain localised plasmon resonances, conferring them unique optical properties that find a wide range of potential applications.[1–7] A remarkable example is surface-enhanced spectroscopy (Raman, but also fluorescence) of molecular species in close proximity to a metal surface.[8,9] The nanoparticles act as resonant antennas for light, funnelling and amplifying the electromagnetic field, resulting in dramatic enhancements of the rate of excitation and re-emission of light by molecular species.[10] This process was recently probed at a more basic level with a direct access to the influence of the metal nanoparticle on light absorption by dye molecules.[11,12] The observed modification of absorbance differs from molecule to molecule and can originate from a variety of effects. First, some molecules may undergo "chemical" modifications in contact with a metal surface;[13–15] as their electron distribution is slightly redistributed the absorption of light can display measurable spectral shifts. This type of effect is highly molecule-dependent. Second, one may expect changes in absorbance of a more electromagnetic nature: it is well known that the presence of a metallic surface can substantially affect the radiation of a classical dipole;[10,16] this may cause enhancement or quenching as commonly studied in the context of plasmonics, but also redirection of radiation and spectral shifts. The latter may also arise from dye–dye interactions, through electromagnetic coupling between induced dipoles.[17,18] In order to elucidate the exact physical origin of the observed modified absorption, it is necessary to disentangle the different types of mechanisms. Classical electromagnetic (EM) theory can be used to model the effects of both dye–dye interactions (including J- or H-aggregates) and of electromagnetic modes supported by the nanoparticle on the optical properties of adsorbed dye layers. The former is well understood on flat films[19] and was more recently studied for spherical shells.[17] For the latter, the most common model considers the dye layer as an isotropic medium with an effective dielectric function accounting for the dye resonance.[20–27] The EM problem is then solved with a given computational framework, such as Mie theory for spheres,[23,26,27] quasi-static approximations[22–24,28] (for spheroids), or FDTD,[29,30] among others. Although successful at describing qualitatively the experiments, (including anti-crossing of resonances[21,25]), such

School of Chemical and Physical Sciences, Victoria University of Wellington, PO Box 600, Wellington, New Zealand. E-mail: baptiste.auguie@vuw.ac.nz; Fax: +64-04-4635237; Tel: +64-04-463 5233 x8987

†Electronic supplementary information (ESI) available: Coupled-dipole equations; detailed description of the generalised coupled dipole method; model for the dye polarisability; self-reflected field in the planar electrostatic approximation; effect of the dye orientation and coverage uniformity. See DOI: 10.1039/C9NR01304K

‡The MacDiarmid Institute for Advanced Materials and Nanotechnology.

a phenomenological model of the dye layer has several limitations. First, it does not take explicitly into account the dye surface concentration (affecting dye–dye interactions), which means that the effective dielectric function is empirical and not derived from the bare optical absorption and dye surface coverage. This makes it difficult to relate spectral changes to their underlying microscopic origin. Second, such *ad hoc* effective medium models do not generally account for the anisotropy of the optical response of the molecular layer, which can be quite strong for dyes that typically adsorb on a metallic surface with a well-defined orientation (for example often flat for planar organic dyes[31]). Despite recent attempts at addressing these problems,[18] it is still not clear whether an effective medium shell model, even improved, would be capable of reproducing all the features of such a system. In any case, an improved effective medium model would need to be benchmarked against a more realistic microscopic model.

Here we develop such a microscopic model for the theoretical description of classical electromagnetic effects for molecular dipoles adsorbed on a spherical core particle. Our model is based on a rigorous solution of the Maxwell equations combining a coupled-dipole description of the interaction of light with multiple dye molecules, with the Mie theory to describe the multipolar contributions from the core nanoparticle to the combined system. For the sake of illustration, we focus on the specific case of dye molecules surrounding a metal sphere, with the molecular absorption detuned from the plasmon resonance, in line with recent experiments[11] (ESI Fig. S1†). The theoretical framework is however much more general, and could readily be applied to other types of emitters or nanoparticles,[32] to dielectric nano-resonators,[33] and also in the context of strong coupling,[29,34] superradiance,[35] Föster resonant energy transfer,[36,37] and related effects involving near-field electromagnetic coupling between emitters in the vicinity of a nanoparticle.[38]

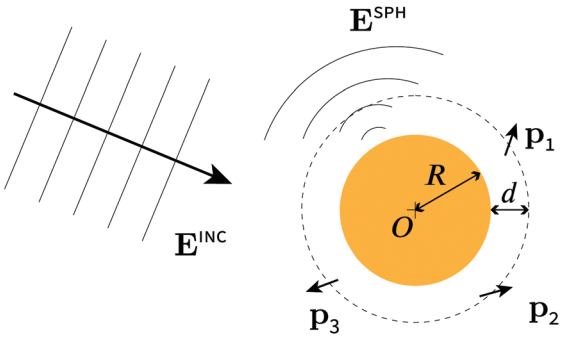

Fig. 1 Schematic representation of the light scattering problem under study. An incident plane wave with associated electric field $\mathbf{E}^{\mathrm{INC}}$ impinges on a spherical nanoparticle of radius R surrounded by polarisable dipoles in arbitrary positions and orientations at a distance d above the sphere. Each dipole responds to a net exciting field that comprises the incident plane wave, the scattered field from the sphere $\mathbf{E}^{\mathrm{SPH}}$, and the scattered field from all neighbouring dipoles in the presence of the sphere.

1. Theory

We consider the situation depicted in Fig. 1, with a collection of N point electric dipoles $\mathbf{p}_i$ located at $\mathbf{r}_i$ and embedded in a homogeneous, non-absorbing, isotropic and non-magnetic infinite medium characterised by a real dielectric function ε_1. This discrete collection of point dipoles represents polarisable molecules surrounding a spherical core nanoparticle, characterised by a dielectric function ε_2. The combined scatterer (dipoles + sphere) is subject to an incident electric field $\mathbf{E}^{\mathrm{INC}}$, taken here as a plane wave. The response of each point dipole $\mathbf{p}_i$ is assumed local and linear and described by a polarisability tensor $\overline{\overline{\alpha}}_i$ (possibly different for each molecule) as $\mathbf{p}_i = \overline{\overline{\alpha}}_i \mathbf{E}_i$, where $\mathbf{E}_i$ denotes the net electric field at the position $\mathbf{r}_i$.

The rigorous solution of this electromagnetic problem in the absence of the sphere falls in the realm of the coupled-dipole method[39–41] and presents many similarities with the popular Discrete Dipole Approximation (DDA).[42,43] The presence of the embedding medium ($\varepsilon_1 \neq 1$) adds a number of complications due to the difference between microscopic and macroscopic fields and the related local field correction. As several definitions are possible to account for these, we provide a brief summary of our implementation of the coupled-dipole method in a medium in section S2 (ESI†). We will now generalise this approach to account for the sphere. We note that a possible alternative approach to the problem would be to use the DDA framework to discretise the nanoparticle and consider its interaction with the surrounding molecular dipoles.[44] Such an approach would meet considerable difficulties for the configuration we consider. The DDA generally discretises scatterers in cubic lattices of point dipoles, with isotropic polarisability. In order to accurately reproduce the optical response of metal nanoparticles, a very large number of dipoles would be required, and combining anisotropic dipoles at arbitrary positions with the DDA model of the nanoparticle would be difficult. In addition, the cubic discretisation of the particle shape introduces an artificially rough surface. Since we are considering molecular dipoles at a very close distance from the nanoparticle, of the order of the discretisation size, the dipole–particle interaction would not be accurately described, as artefacts of near-field amplitude and polarisation would be introduced. For these reasons we chose to develop an original hybrid method, combining the coupled-dipole model with Mie theory to describe rigorously and efficiently the nanoparticle's response.

1.1 Generalised coupled-dipole equations

The electric field $\mathbf{E}_i$ may be formally decomposed as the sum of the incident field $\mathbf{E}_i^{\mathrm{INC}}$, plus the incident field scattered by the sphere $\mathbf{E}_i^{\mathrm{SPH}}$, and the total field scattered by the other dipoles. The self-consistent system of generalised coupled-dipole equations thus takes the form

$$\mathbf{E}_i = \mathbf{E}_i^{\mathrm{INC}} + \mathbf{E}_i^{\mathrm{SPH}} + \sum_{j \neq i} \overline{\overline{G}}_{ij} \overline{\overline{\alpha}}_j \mathbf{E}_j + \sum_{\forall j} \overline{\overline{S}}_{ij} \overline{\overline{\alpha}}_j \mathbf{E}_j, \qquad (1)$$

where the Green tensor describing the coupling between dipoles i and j is decomposed in two contributions: $\overline{\overline{G}}_{ij} = \overline{\overline{G}}(\mathbf{r}_i, \mathbf{r}_j)$ expresses the standard dipole–dipole interaction between dipoles i and j in an infinite homogeneous medium,[43] while the additional contribution $\overline{\overline{S}}_{ij}$ describes the dipole–dipole interaction mediated by the sphere, calculated using generalised Mie theory (see ESI sections S2 and S3† for explicit formulas). We note that $\overline{\overline{S}}_{ii}$ is non-zero, and corresponds to the self-reaction of dipole i due to the sphere (akin to a "reflected field" acting back on the dipole itself[45,46]). As in the standard coupled-dipole formalism, optical reciprocity imposes the symmetry $\overline{\overline{G}}_{ji} = \overline{\overline{G}}_{ij}^{\mathrm{T}}$, however the product $\overline{\overline{G}}_{ij}\overline{\overline{\alpha}}_j$ breaks this symmetry for an arbitrary pair of polarisabilities $\overline{\overline{\alpha}}_i$ and $\overline{\overline{\alpha}}_j$ (*e.g.* for different molecules, or anisotropic identical molecules rotated to different orientations). The coupled-dipole equations are often presented in a different form, in terms of the dipole moments $\mathbf{p}_i$, but this equivalent formulation in terms of the self-consistent macroscopic fields $\mathbf{E}_i$ is more suitable for the purpose of this work, as the solution of eqn (1) does not involve the matrix inverse $\overline{\overline{\alpha}}_i^{-1}$, which is problematic for uniaxial molecules.

This linear system of $3N$ equations is cast in matrix form by grouping the fields $\mathbf{E}_i$, $\mathbf{p}_i$, $\mathbf{E}_i^{\mathrm{INC}}$ and $\mathbf{E}_i^{\mathrm{SPH}}$ into column vectors of length $3N$. The matrix equation then reads,

$$\overline{\overline{A}}\mathbf{E} = \mathbf{E}^{\mathrm{INC}} + \mathbf{E}^{\mathrm{SPH}}, \tag{2}$$

where $\overline{\overline{A}}$ is the full interaction matrix obtained by combining the 3×3 Green tensors $\overline{\overline{G}}_{ij}$ and $\overline{\overline{S}}_{ij}$,

$$\overline{\overline{A}}_{ij} = \begin{cases} \overline{\overline{I}}_3 - \overline{\overline{S}}_{ii}\overline{\overline{\alpha}}_i & i = j, \\ \overline{\overline{G}}_{ij}\overline{\overline{\alpha}}_j - \overline{\overline{S}}_{ij}\overline{\overline{\alpha}}_j & i \neq j. \end{cases} \tag{3}$$

Solving eqn (2) numerically provides the self-consistent macroscopic fields $\mathbf{E}_i$ from which we can derive the dipole moments $\mathbf{p}_i$, as in the standard coupled-dipole theory.

In order to allow direct comparison of the solution of eqn (2) with experimental results, we seek far-field cross-sections that describe the entire coupled system (sphere and dipoles) in response to an incident plane wave. While the standard coupled-dipole expressions could be used to calculate the absorption, scattering and extinction from the set of dipole moments in response to the incident field, it is important to remark that the results would correspond to a quantity that is not directly accessible to experiments – what is measured is the response of the combined system, namely dipoles and sphere.

The total cross-sections can be obtained following the generalised Mie theory formalism, now considering the self-consistent dipole moments as sources of radiation, expanded into a common basis of vector spherical wavefunctions, together with the incident plane wave, and calculating the total scattered field from this combined excitation. These formulas give the far-field cross-sections of the combined system (see ESI section S3† for details).

In some situations, for example at low dye concentrations,[11] the dye contribution may be hidden in the much stronger optical response of the metal colloid. In such cases, one can subtract the corresponding cross-section for the bare sphere (with no dipoles, *i.e.* solving a different scattering problem) to obtain the differential cross-section, for example for absorption, σ_{abs},

$$\sigma_{\mathrm{abs}} = \sigma_{\mathrm{abs}}^{(\mathrm{sphere+dipoles})} - \sigma_{\mathrm{abs}}^{(\mathrm{sphere\ only})}. \tag{4}$$

It is important to note that because of the coupled nature of this system, σ_{abs} is not in general equal to the absorption cross-section of the induced dipoles only (which would be much simpler to calculate), as the dipoles also induce currents within the nanosphere that contribute to the total absorption.

We will refer to this approach as the generalised Coupled-Dipole Method (GCDM), which we apply to specific model systems in the remainder of this article. All calculations were performed using Matlab on a high-end PC; the limiting factor in our implementation is the maximum number of dipoles (up to several thousand), dictated by the size of the linear system (eqn (2)).

2 Results

The presence of a core sphere adds considerable complexity to the already-rich optical response of interacting dye molecules in arbitrary 3D configurations, which we recently investigated.[17] The core particle, especially when metallic or of high refractive index, can substantially modify the intensity and polarisation of the local field exciting the dipoles, and also their coupling. The plasmonic effect associated with the increased field intensity can be studied within standard Mie theory and is well documented, as it is the primary enhancement mechanism in surface-enhanced spectroscopies.[9] We will here instead focus on the additional effects that are not captured in standard electromagnetic models but arise naturally within our generalised coupled-dipole model namely: the self-reflected field (image dipole effect), dye–dye interactions, and dye orientation effects.

2.1 Model system

To limit the parameter space, we focus on a specific system where a variety of interactions are clearly illustrated. The core particle is chosen as a silver nanosphere, with dielectric function ε_2 taken from ref. 9, embedded in water (of dielectric constant $\varepsilon_1 = 1.33^2$). This choice of particle introduces plasmon resonances with dramatic effects on the optical response, and is directly relevant to many experiments. We assessed the effect of the sphere radius in the range R = 10 nm–30 nm and found that, beside the standard plasmonic effect on the field enhancement (red-shift of the resonance and radiative damping), the nanosphere radius does not impact any of our conclusions in this range. Larger radii do however significantly increase the computational challenge at high dye coverage because of the substantial increase in the number of dipoles. For example, at a coverage of ρ = 1 dye per nm^2, the simulations involve ~2500 dipoles for R = 14 nm and more than

11 000 for R = 30 nm. With the exception of Fig. 7, where we attempt to match experimental results more closely, the results presented here are for a nanosphere radius of R = 14 nm for which the main dipolar plasmon resonance is located at 397 nm.

For the dye, we restrict our study to isotropic and uniaxial polarisability tensors, which again covers many relevant experiments. The frequency-dependent polarisability is taken as a single Lorentzian lineshape to easily identify shifts and/or broadening of the peak. For any quantitative study of the dye–dye interaction, the magnitude of the polarisability is a crucial parameter and we therefore set it to match a specific experimental example, the dye Rhodamine 6G. Explicit expressions for the polarisability are given in ESI section S3.† The dye resonance at 526 nm is offset with respect to the plasmon resonances around 400 nm to avoid strong interactions between the plasmon and dye resonances. The strong coupling regime would certainly be interesting in its own right and can be studied in detail using our generalised coupled-dipole model, but it makes it harder, or indeed impossible, to disentangle the spectral modification in the dye's response from that of the combined system. We therefore choose to first understand the variety of EM effects (reflected field, dye–dye interaction, dye orientation) in the weak coupling regime, before attempting to interpret the model's predictions in a strong coupling regime with the plasmon resonance.

We also choose to focus on a sub-monolayer, low-coverage regime, which arguably yields more physical insight than higher concentrations dominated by multilayer effects. However, the optical response of the dyes is then barely visible in the much stronger NP response. For this reason, we will consider differential absorption spectra or cross-sections obtained from subtracting the bare NP spectrum from the dye-NP spectrum. When the dye and plasmon resonances are not interacting, this differential spectrum provides an insight into the modified absorbance of the dye on the colloid and may be accessed experimentally,[11] enabling a direct comparison.

2.2 Self-reflected field and image-dipole effect

Before considering interactions between multiple dyes, it is instructive to revisit the response of a single dipole near the sphere. This is a standard microscopic model for the electromagnetic enhancement in surface-enhanced spectroscopies.[18,47] The sphere's response is typically calculated using the Mie theory and the resulting electric field is then used to deduce the induced dipole and its optical response. This approach however ignores the self-reflected field, *i.e.* the field created by the dipole and reflected by the sphere, which is also not included in the effective-medium approximation.[11] Our generalised coupled-dipole model does take into account this interaction through the terms $\bar{\bar{S}}_{ii}$. This self-reflected field can also be investigated simply by considering a single dipole, for which the reflected field is obtained as $\mathbf{E}^{\mathrm{SR}} = \bar{\bar{S}}_{11}\mathbf{p}_1$. We note that this self-reaction, sometimes referred to as image-dipole effect, was considered early-on as a possible mechanism for SERS enhancements[48–50] and has been revisited more recently in the context of surface-enhanced Raman[51,52] and fluorescence[53] processes. In all these cases, the self-reflected field was computed in the electrostatic limit assuming that the dipole sits at a distance d from a planar metal surface. This simpler EM problem can be solved using the method of images,[54] where the reflected field is given by the field created by the dipole image evaluated at the real dipole's position (see ESI section S5† for full expressions).

Such predictions are compared in Fig. 2 with the exact results derived from the GCDM. We see that the electrostatic-planar approximation is rather accurate in the range of parameters investigated here. In fact, further calculations revealed that the small discrepancy can be largely attributed to the contribution of the sphere to the total absorption in the GDCM, which is not considered in the simple image-dipole model.

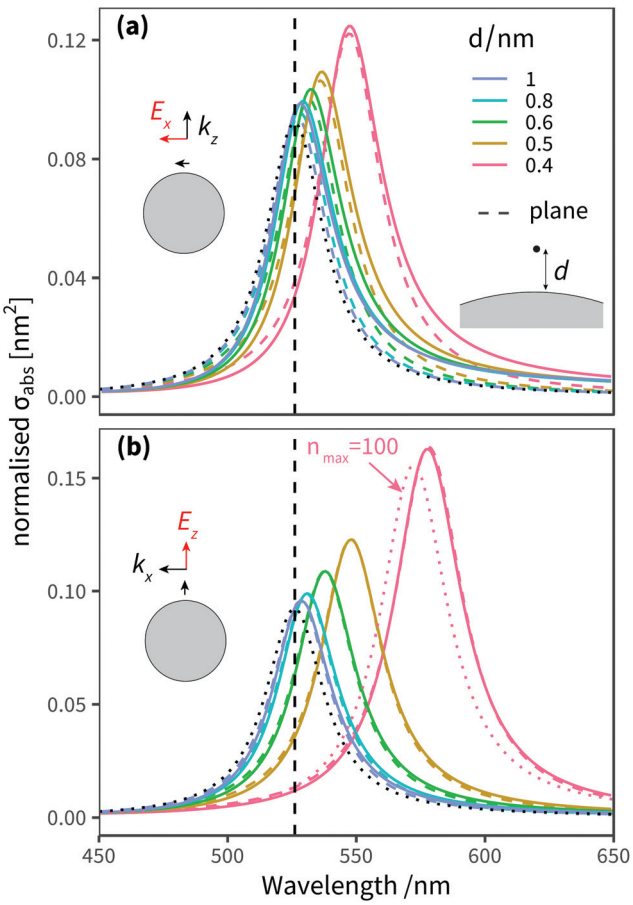

Fig. 2 Image dipole effects: Differential absorbance spectra for a single polarisable dipole at different distances d from a 14 nm radius silver sphere. We consider a uniaxial polarisability either perpendicular (a) or parallel (b) to the sphere surface, illuminated by an incident plane wave. The GCDM predictions with maximum multipolar order n_{max} = 500 (solid lines) are compared with those of a dipole-near-a-plane in the electrostatic approximation (eqn (S21)–(S23)† – dashed lines). The cross-sections predicted from GCDM are scaled down by the local field enhancement factor at the dipole position, to facilitate the comparison with the planar dipole-image case. We also show the GCDM prediction for n_{max} = 100 (pink dotted line, for d = 0.4 nm) to highlight the need for large n_{max}, especially at short distances d from the surface.

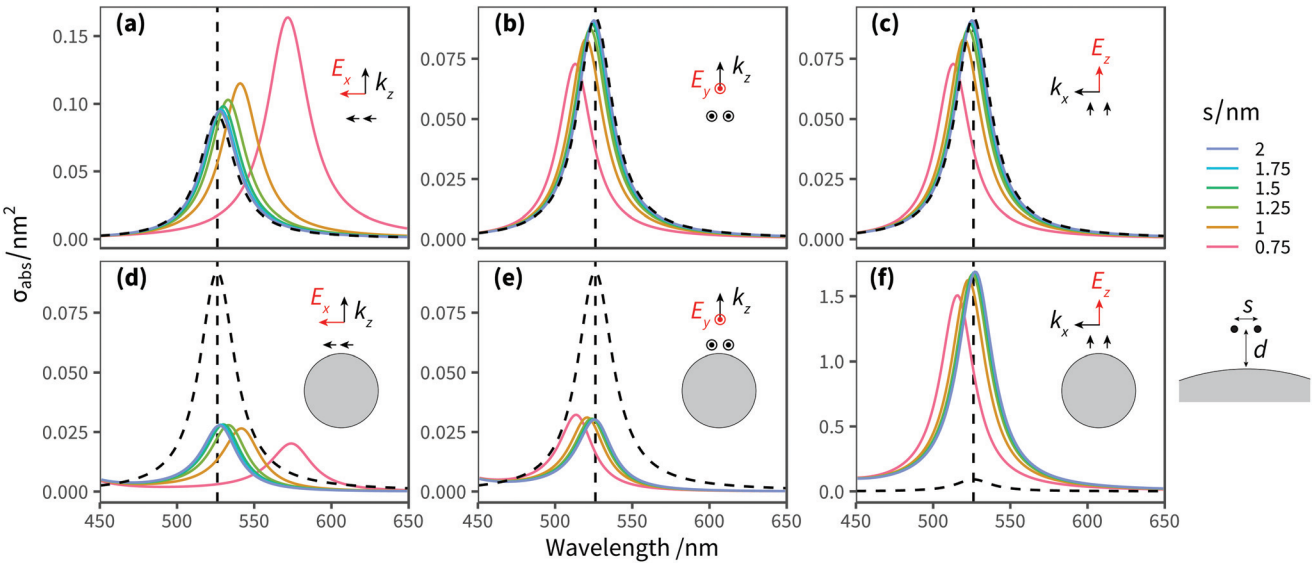

Fig. 3 Differential absorbance spectra for a dimer of isotropic dipoles with varying separation *s*. (Top) The dimer is illuminated by an incident plane wave, and no sphere is present. Three illumination directions are considered: E_x (a), E_y (b), E_z (c). (Bottom) Corresponding spectra when the dipoles are placed at a distance d = 1 nm above the surface of a 14 nm radius silver sphere. The dotted black line in each panel shows the reference absorption spectrum of a single isolated dye in the incident medium.

This good agreement suggests that the "reflected" field is not affected much by the curvature of the sphere, the sphere's localised plasmon resonances, or retardation effects. This is an important result as it suggests that this simple approximation may equally apply to a wide range of other particle shapes. We can also point out two other important observations:

• The accurate calculation of the reflected field for a sphere requires the inclusion of a large number n_{max} of multipoles (see Fig. 3b). A similar truncation is in fact required to compute the field created by one dipole at another location *via* the interaction with the sphere, which means that a large n_{max} must be used for all our calculations, especially for the lowest d.

• One advantage of the GCDM over the planar electrostatic approximation is that it also predicts the effect of the single dipole on the absorbance/resonance of the sphere. This is evident in the differential absorption spectrum in the derivative like spectral shape around the plasmon resonance, which reflects the plasmon resonance shift resulting from the presence of a single polarisable dipole on the sphere surface (not shown here, but visible in Fig. 5 for example).

2.3 Dimer of interacting dyes

We now focus on dye–dye interactions, which are expected to become increasingly important as the coverage increases. In order to better disentangle the various electromagnetic interaction mechanisms, we first consider a minimal system comprising a dimer of uniaxial dipoles placed symmetrically about the *z* axis at a distance d above the sphere's surface, with inter-dipole separation s (Fig. 3). The dipole–dipole and dipole–sphere coupling terms are strongly orientation-dependent, and we therefore distinguish 3 different dipole orientations with corresponding polarisation/incidence for the incident electric field. We note that for sub-wavelength systems the incident wave's direction of propagation is not as important as that of the electric field, as retardation effects play but a minor role. It is instructive to compare the response of a dimer as a function of separation with and without the sphere (top *vs.* bottom rows). The dashed black line, identical in all panels, shows the single isolated dye's Lorentzian lineshape for reference. Without the sphere, we confirm the well-characterised red-shift and blue-shift of the absorption peak as the separation between dipole decreases,[17] corresponding to J-aggregate and H-aggregate configurations (head-to-tail *vs.* side-by-side induced dipoles, respectively).[55]

Such spectral shifts are retained when the silver sphere is added to the simulations, however with important changes in intensities. Head-to-tail induced dipoles are parallel to the metal surface in this configuration and therefore experience a quenching in the differential absorbance (panel (d)), as the local electric field near the surface of a good metal can only have a very small tangential component (vanishing in the limit of a perfect conductor). Side-by-side induced dipoles may be parallel or perpendicular to the metal surface (panels (e) and (f), respectively), and the presence of the sphere serves to quench (respectively enhance) the differential absorption cross-section; this amplification is due to the local field enhancement factor $|E_\perp|^2/|E_0|^2$ or $|E_\parallel|^2/|E_0|^2$ experienced by molecules near the metal surface.[9,31]

For the fixed distance d = 1 nm considered in Fig. 3 the predicted spectral shifts are very similar with and without the sphere, suggesting that the sphere's contribution is largely to enhance (or quench) the local field, but that it is not substantially affecting the dipole–dipole interaction. In other words,

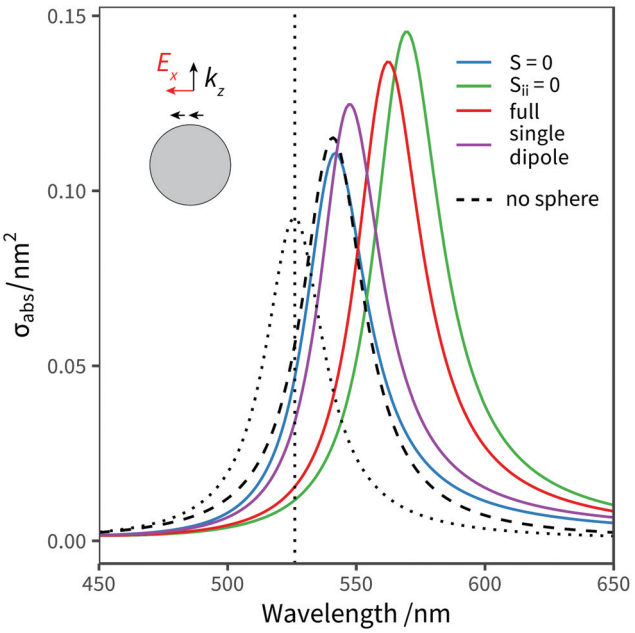

Fig. 4 Influence of the sphere-mediated Green tensor $\bar{\bar{S}}$ to the optical response. We compare the full solution of the electromagnetic problem of eqn (1) for a parallel dimer tangential to the sphere, with s = 1 nm, d = 0.4 nm (red curve) to the predictions obtained by setting $\bar{\bar{S}}$ = 0 (blue curve), or only the self-reflected contribution (diagonal blocks $\bar{\bar{S}}_{ii}$ = 0, green curve). For reference, the dotted line is the isolated dipole's response in the medium, the dashed line the response of the same dimer without the sphere, and the purple curve corresponds to a single dipole at a distance d = 0.4 nm from the sphere, giving a measure of the image dipole shift.

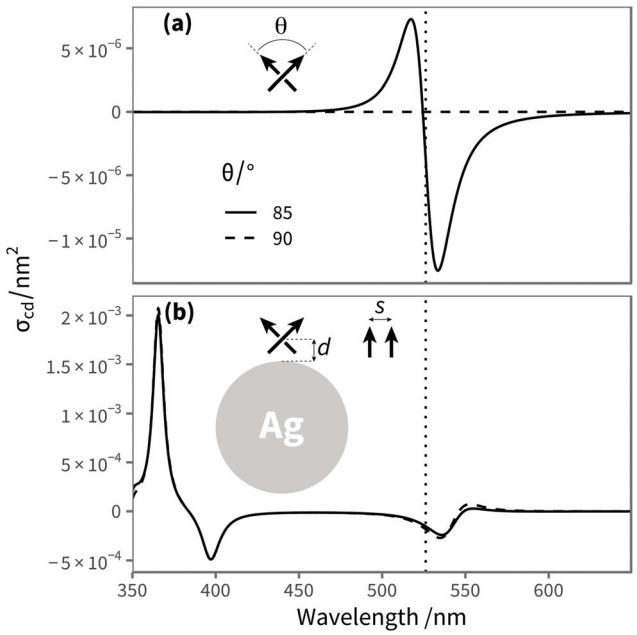

Fig. 5 Orientation-averaged circular dichroism calculations for a dimer of uniaxial dyes separated by s = 0.8 nm, with a dihedral angle θ = 85° or θ = 90°. (a) Simulated circular dichroism for the isolated dimer. With θ = 90°, the dimer is achiral, resulting in zero circular dichroism. (b) Same dimer, situated at a distance d = 0.8 nm above a 14 nm-radius silver sphere.

the Green tensor's contribution due to the sphere, $\bar{\bar{S}}_{ij}$, is relatively small in comparison to the free-space coupling term $\bar{\bar{G}}_{ij}$.

This observation is by no means general, but merely reflects the relatively large separation (d = 1 nm) between dipoles and sphere. The effects of a lower distance d = 0.4 nm are illustrated in Fig. 4, where we compare the relative strength of the free-space and sphere-mediated coupling terms, $\bar{\bar{G}}$ and $\bar{\bar{S}}$, respectively, on a dimer with separation s = 1 nm. The full electromagnetic response (red curve) requires in this case a full account of all terms, namely: (i) the dipole–dipole interaction in the medium ($\bar{\bar{G}}$) introduces a shift from the isolated dipole response (dashed curve *vs.* dotted curve); (ii) the single dipole near the sphere experiences a substantial shift due to the dipole image effect ($\bar{\bar{S}}_{ii}$, purple curve); (iii) the combination of both effects, and cross-coupling mediated by the sphere ($\bar{\bar{S}}_{ij}$) also contributes to the interaction. We can artificially disable the sphere-mediated coupling $\bar{\bar{S}}$ entirely (blue curve), or only the diagonal blocks $\bar{\bar{S}}_{ii}$ responsible for self-reaction (green curve), to confirm that all terms contribute. We note that the dipole-image effect alone cannot explain the spectral shifts of the dimer: in other words, we cannot consider the response of the dimer near the sphere as two effective dipoles renormalised by their respective image dipole. The sphere-mediated coupling term $\bar{\bar{S}}$ is required to account for the cross-coupling between the two dipoles, not just the individual sphere-mediated self-reaction.

Finally, the presence of a metal sphere may also affect dipole–dipole interactions through modification of the field polarisation. This is particularly striking in circular dichroism (Fig. 5), which is extremely sensitive to relative orientations.[56,57] A chiral dimer of dipoles is a simple model for optical activity,[58,59] which can reveal the physical origin of the typical bi-signated Cotton effect observed in circular dichroism spectroscopy of molecules with several chromophores,[60] or, more recently, artificial assemblies of metal nanoparticles.[61,62] In Fig. 5(a) we consider a dimer of uniaxial molecular dipoles, without the sphere, and calculate the orientation-averaged circular dichroism by taking the difference in absorption cross-sections for left- and right-circularly polarised light. The dimer with a dihedral angle of θ = 90° is achiral, as it allows two planes of symmetry, and consequently the circular dichroism vanishes. For a slight dissymmetry, with θ = 85°, a characteristic bi-signated lineshape is predicted.[56] In contrast, the same dimer placed above a metal sphere can break this symmetry even for θ = 90° and present a strong circular dichroism signal (Fig. 5(b)), interestingly with a reversed spectral shape. The disymmetric dipole–dipole interaction with left- and right-circularly polarised light is strongly affected by the coupling mediated by the sphere; in turn, the dipoles also induce a strong circular dichroism response in the spectral region of the plasmon resonance (350–400 nm), which has been suggested as a promising mechanism of enhancement of naturally-weak optical activity signals.[63,64]

With these different contributions distinguished, we may now summarise how the core particle affects the dipole–dipole interaction in this core–shell configuration. Besides the local-field enhancement (or quenching) of absorption, there are two aspects to the dipole–sphere interaction: first, a single dipole will experience an interaction *via* its self-field, "reflected" by the sphere. For distances below 1 nm, this effect rises very rapidly and causes a dramatic red-shift. The second effect, more subtle, is to modify the inter-dipole interaction through the additional field mediated by the sphere. The net result is to modify the spectral shift due to the dipole–dipole coupling and the field polarisation/orientation effects.

2.4 Spherical shells of interacting dyes

Although dimers with specific relative orientations can capture the essential physics and predict red or blue shifts depending on the electromagnetic interaction between induced dipoles, a quantitative description of a large collection of dye molecules with specific relative positions and orientations requires an explicit account of all their pair-wise interactions. In a recent study[17] we highlighted the importance of collective effects in a complex 3-dimensional geometry such as a spherical arrangement of anisotropic dipoles. This situation carries, with additional complexity, to the case of core–shell structures where the core particle can strongly influence the local field intensity, polarisation, as well as self-reaction and dipole–dipole coupling.

We illustrate in Fig. 6 the effect of a silver core particle on the differential absorption spectrum of three configurations of dye molecules, with idealised representative adsorption geometries: isotropic dipoles; uniaxial dipoles pointing radially; uniaxial dipoles oriented tangentially at random. Panels (a)–(c) consider the dipole–dipole interactions in the spherical shell geometry without any core particle. The results for a shell of isotropic dipoles (a) closely resembles the predictions of a simple effective-medium approximation, namely the splitting of the main absorption line with increasing dye concentration into a main red-shifted peak, associated with head-to-tail interactions between neighbouring induced dipoles, and a weaker blue-shifted band associated with side-by-side interactions.[17] This interpretation is supported by the simpler spectral response exhibited by uniaxial dipoles: the radially-oriented dipoles are locally almost parallel (panel (b)), and show only a blue shift as the surface concentration increases; similarly, the tangentially-oriented dipoles favour a head-to-tail interaction between near neighbours (panel (c)).

The bottom panels (d)–(f) introduce a 14 nm radius silver sphere at the centre of the shell of dipoles. The core–shell separation is d = 1 nm, chosen for consistency with previous work.[11,17] Qualitatively, the coverage-dependent spectral shifts follow the same trends as in the void-core situation except for the predicted intensities. These are strongly affected by the presence of the metal core because of the wavelength and polarisation dependence of the local field enhancement factor, as for the dimer discussed earlier. The predicted spectral shifts are also affected by the presence of the sphere but to a lesser extent. We nevertheless emphasise again that these shifts can only be quantitatively predicted by a model where all electromagnetic interactions are duly accounted for, including dye–dye interactions and their orientation/polarisation dependence. Future effective medium shell models for this problem could in fact be tested by their ability to reproduce the predictions of Fig. 6.

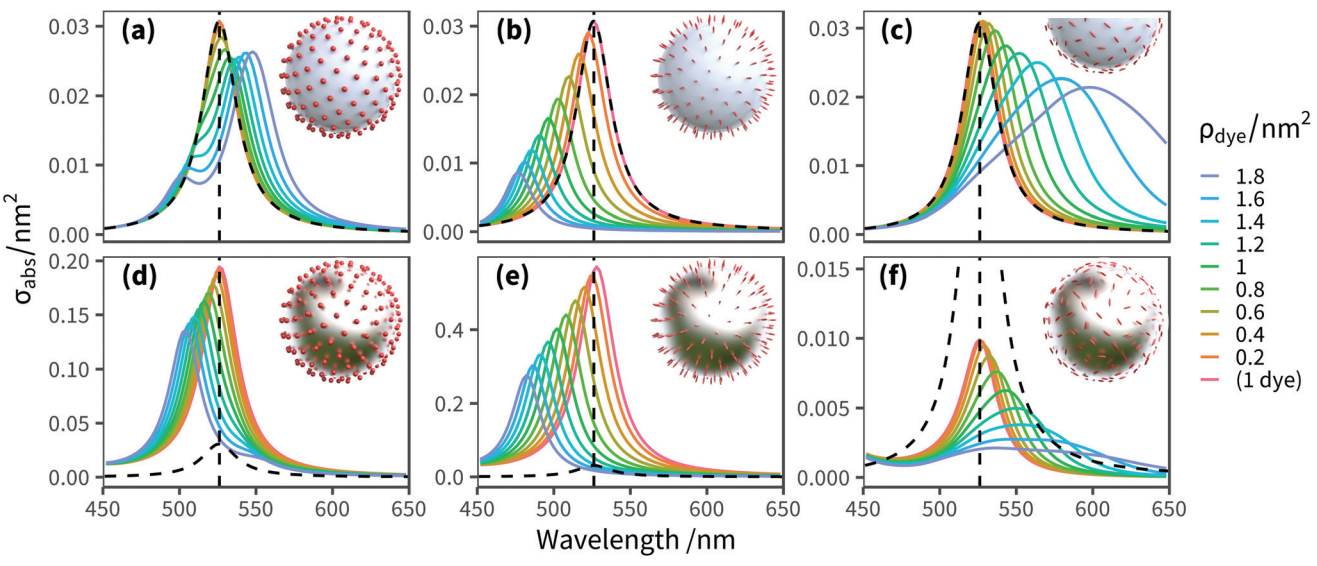

Fig. 6 Effect of a metal core particle on the dipole–dipole interaction between dye molecules at a distance d = 1 nm in a spherical core–shell geometry. (Top) Void shell results (no core). (a) Isotropic dipoles; (b) uniaxial dipoles, radially-oriented; (c) uniaxial dipoles, tangentially-oriented at random. (Bottom) Corresponding simulated spectra with a 14 nm radius silver spherical core. The dashed black line common to all panels shows the free dye's absorption spectrum in the medium, for reference.

3 Comparison to experiments

Using the experimental approach described in ref. 11, we can measure the differential absorbance cross-section of dye molecules adsorbed onto metallic nanoparticles. We focus specifically on the case of Rhodamine 6G (RH6G) adsorbed on Cl^--ion-coated 30 nm-radius silver nanospheres, as previously studied.[11] Because of electrostatic interaction, RH6G adsorbs efficiently on the nanoparticles.[65] Assuming 100% adsorption efficiency, we can estimate the dye coverage from the ratio of dye concentration c_d to NP concentration c_{NP}: $\rho = (c_d/c_{NP})/(4\pi R^2)$. The dye–dye interaction effects discussed earlier can therefore be evidenced experimentally by varying the dye concentration. The two main parameters that can be adjusted in the theory (and are not easily determined by experiments) are the distance d to the surface, assumed constant, and the orientation of the dye, whose optical response is assumed uniaxial. A detailed experimental investigation is outside the scope of this work, but we nevertheless show in Fig. 7 representative experimental results (see ref. 11 for full experimental details) along with the predictions of the GCDM theory. Note that the comparison with experimental data in this section is not aimed at drawing definite conclusions, but rather at highlighting the diversity and richness of mechanisms that need to be considered when interpreting them. This reinforces the importance of a model, like the GCDM, that is able to capture all these effects under one theoretical framework.

The modified absorption spectrum at the lowest coverage (red curve in Fig. 7a) is red-shifted to 538 nm compared to the original absorption of RH6G in water (dotted line), which peaks at 526 nm. This might be explained by the image dipole effect, but we show in Fig. 7a (blue curve) that adjusting the distance to d = 0.5 nm to match the observed spectral shift of the main peak does not reproduce well the spectral lineshape. In particular, the high-energy shoulder does not shift enough and the ratio of peak intensities disagrees with the experimental observations. An alternative explanation is a chemical change in the molecule itself, *i.e.* a modification of the electronic structure and therefore polarisability of the dye upon adsorption of the metal. To study the coverage dependence, we therefore assume the following strategy: we choose a distance d = 1 nm to minimise the image-dipole shift and empirically define a modified polarisability (dashed line), labelled RH6G*, that is artificially shifted to reproduce the low-concentration experimental spectrum. The resulting prediction (Fig. 7a, purple curve) is by construction close to the experiment at the lowest coverage, except around 450 nm where the predicted differential absorbance is negative (see discussion below). We ensured that the oscillator strength of RH6G* is the same, so the magnitude of the absorption spectrum can only be adjusted to match experiments by specifying the orientation with a tilt angle of $\theta = 75°$ with respect to the normal. We note that this is different to another recent indirect inference of the orientation of RH6G on silver colloids,[66] where a more normal orientation was deduced. This discrepancy might be attributed to the different halide co-ion or to the aggregation state of the

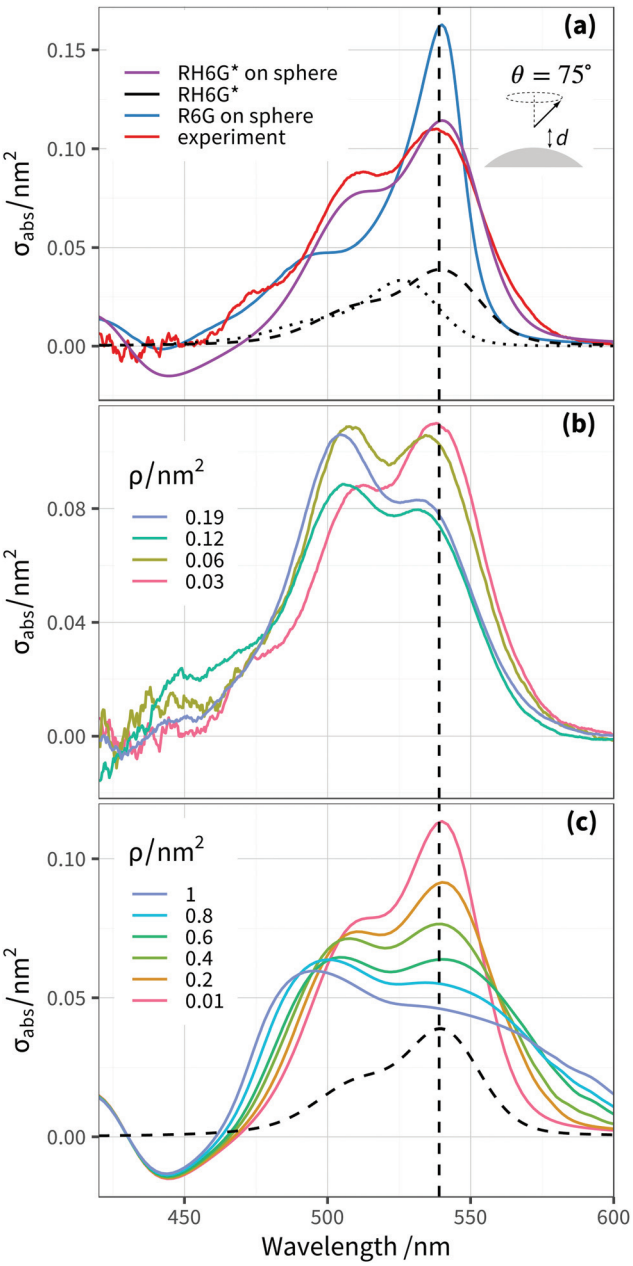

Fig. 7 Comparison of predicted differential absorbance spectra with experiments. (a) The lowest-concentration data (red curve) are used to infer the isolated-dye response when adsorbed onto silver colloids. To match the observed spectral shift from the bare dye (dotted line), the blue curve considers a single dipole oriented at 75 degrees from the sphere surface, and positioned at a distance d = 0.5 nm, adjusted so that the image-induced shift matches the observed position of the main peak. The purple curve considers instead a single dipole at a distance d = 1 nm (negligible image dipole effect), but with a modified polarisability, corresponding to the dashed curve (labelled RH6G*). (b) Experimental differential absorbance spectra as a function of surface concentration. (c) Predicted differential absorbance spectra as a function of surface concentration. The dipoles are positioned randomly with a minimal exclusion distance of 0.7 nm, and oriented at 75° from the normal.

colloid: Br^--aggregated colloids in ref. 66 whereas the low Cl^- concentration does not induce any aggregation in our experiments.

With this new polarisability and tiltangle, we can now predict the concentration-dependence of the differential absorbance spectrum, and compare it to the experimental observations. The latter are shown in Fig. 7b, where they have been normalised by the number of adsorbed dyes. We note that a baseline correction is applied to these differential spectra, which implicitly assumes that the spectra approach zero around 450 nm.[11] Nevertheless, we observe a clear increase in the relative intensity of the short-wavelength absorption peak as the coverage increases, which should be reproduced by the model. The GCDM's predictions are shown for comparison in Fig. 7c (the tilt-angle dependence of these predictions and the effect of uniform *vs*. random coverage are also further discussed in section S5†). These predictions were obtained with a sphere radius of R = 30 nm in order to describe more accurately the local field enhancement factor and its spectral dependence.§ Overall the model satisfactorily predicts the observed spectral changes as a function of surface coverage. The relative intensity of the main peak and the high-energy shoulder are seen to evolve in good agreement with the observations. A closer inspection reveals that the model predicts a larger blue-shift of the high-energy peak and an increased broadening of the main peak than observed. Another discrepancy is that the scale of concentrations (or coverage ρ) required to match the spectral changes in the experimental data is substantially larger than expected. A possible interpretation for all these discrepancies is the formation of RH6G dimers on the NP surface. Our simulations assume a relatively homogeneous coverage of the colloids, but in reality the adsorption process may occur more randomly, or even lead to preferential dimerisation. The results presented in Fig. 7c take into account this inhomogeneous coverage with a minimal exclusion distance to avoid non-physical dipole–dipole interactions, and yield a spectral broadening, particularly at the low-energy end. If the dye has a tendency to form dimers on the surface, such aggregates would have a fixed distance, dictated by the interaction energy of the dimer, resulting in better-defined peaks and a faster concentration-dependence of the spectral evolution, as observed in the experiment (Fig. 7b). Although such a conclusion cannot be drawn here from a single set of experimental data, we note that the formation of RH6G dimers on silver nanoparticles was also deduced by others using different type of experiments.[67]

Finally, the model also predicts that differential absorbance should in fact be negative around 450 nm (due to the shift of the dipolar plasmon resonance). This should inform future experiments, as it highlights the need for more reproducible data that do not require a baseline correction.

§ For practical reasons, the simulations were run with a partial coverage of the sphere, to limit the number of dipoles in the simulations[17] (the linear system becomes difficult to solve on a standard PC with more than several thousand dipoles). We ran the simulations with a coverage limited to a spherical cap of 20% and 30% of the full sphere surface, and little difference can be seen. The results are presented for 30%.

4 Conclusions

We have introduced an original electromagnetic model to simulate the optical properties of molecular dipoles in close proximity to a spherical core particle. Our scheme combines the coupled-dipole model, to describe interactions between molecules, with rigorous multipolar interactions mediated by the sphere calculated from generalised Mie theory. In the case of a metal core particle, highly-relevant in surface-enhanced spectroscopies, we predict strong modifications of the dipole–dipole interaction. We applied the model to a simple dimer geometry to highlight the key electromagnetic interaction mechanisms that can be expected to occur in realistic molecule–nanoparticle systems. We followed with a comprehensive exploration of different spherical core–shell geometries of relevance to recent experimental findings, varying the dye concentration, orientation and uniformity in coverage. The results exhibit a rich variety of spectral modifications that cannot be captured by a simple effective-medium approximation for the shell of dyes.

This model is applicable to a much wider range of systems. Molecule–nanoparticle electromagnetic interactions are central to many current research topics, beyond the illustrative examples treated in this work. Of particular interest will be the study of dielectric nano-resonators[33] with high quality factors, the dependence of strong coupling[29,34] on surface coverage and molecular orientation when the core particle sustains a resonance tuned with the molecular resonance, but also the influence of a core particle on superradiance,[35] or Föster resonant energy transfer[36,37] between collections of dipole emitters. The subtle changes in the polarisation properties of the local electric field have also promising applications in the understanding of surface selection rules and surface-enhanced optical activity near nanostructures.

Conflicts of interest

There are no conflicts to declare.

Acknowledgements

The authors thank the Royal Society Te Apārangi for support through a Rutherford Discovery Fellowship (B. A.) and a Marsden grant (E. C. L. R.).

References

1 H. A. Atwater and A. Polman, *Nat. Mater.*, 2010, **9**, 205–213.
2 S. Linic, P. Christopher and D. B. Ingram, *Nat. Mater.*, 2011, **10**, 911–921.

3 Y. H. Jang, Y. J. Jang, S. Kim, L. N. Quan, K. Chung and D. H. Kim, *Chem. Rev.*, 2016, **116**, 14982–15034.
4 S. L. Kleinman, et. al, *Phys. Chem. Chem. Phys.*, 2013, **15**, 21–36.
5 S. Xu, J. Shan, W. Shi, L. Liu and L. Xu, *Opt. Express*, 2011, **19**, 12336.
6 C. M. Galloway, C. Artur, J. Grand and E. C. Le Ru, *J. Phys. Chem. C*, 2014, **118**, 28820–28830.
7 Y. Zhang, S. He, W. Guo, Y. Hu, J. Huang, J. R. Mulcahy and W. D. Wei, *Chem. Rev.*, 2018, **118**(6), 2927–2954.
8 *Surface-Enhanced Vibrational Spectroscopy*, ed. R. Aroca, Wiley-Blackwell, 2007.
9 E. C. Le Ru and P. G. Etchegoin, *Principles of Surface Enhanced Raman Spectroscopy and Related Plasmonic Effects*, Elsevier, Amsterdam, 2009.
10 W. L. Barnes, *J. Mod. Opt.*, 1998, **45**, 661–699.
11 B. L. Darby, B. Auguié, M. Meyer, A. E. Pantoja and E. C. Le Ru, *Nat. Photonics*, 2015, **10**, 40–45.
12 F. Stete, W. Koopman and M. Bargheer, *ACS Photonics*, 2017, **4**, 1669–1676.
13 D. A. Alexson, S. C. Badescu, O. J. Glembocki, S. M. Prokes and R. W. Rendell, *Chem. Phys. Lett.*, 2009, **477**, 144–149.
14 L. Zhao, L. Jensen and G. C. Schatz, *J. Am. Chem. Soc.*, 2006, **128**, 2911–2919.
15 B. N. J. Persson, *Chem. Phys. Lett.*, 1981, **82**, 561–565.
16 G. W. Ford and W. H. Weber, *Phys. Rep.*, 1984, **113**, 195–287.
17 B. Auguié and E. C. Le Ru, *J. Phys. Chem. C*, 2018, **122**, 19110–19115.
18 C. Tang, B. Auguié and E. C. Le Ru, *ACS Photonics*, 2018, **5**(12), 5002–5009.
19 A. Nabetani, A. Tomioka, H. Tamaru and K. Miyano, *J. Chem. Phys.*, 1995, **102**, 5109–5117.
20 G. P. Wiederrecht, G. A. Wurtz and J. Hranisavljevic, *Nano Lett.*, 2004, **4**, 2121–2125.
21 N. T. Fofang, T.-H. Park, O. Neumann, N. A. Mirin, P. Nordlander and N. J. Halas, *Nano Lett.*, 2008, **8**, 3481–3487.
22 W. Ni, *et al.*, *Nano Lett.*, 2010, **10**, 77–84.
23 H. Chen, L. Shao, K. C. Woo, J. Wang and H.-Q. Lin, *J. Phys. Chem. C*, 2012, **116**, 14088–14095.
24 G. Zengin, *et al.*, *Sci. Rep.*, 2013, **3**, 3074.
25 A. E. Schlather, N. Large, A. S. Urban, P. Nordlander and N. J. Halas, *Nano Lett.*, 2013, **13**, 3281–3286.
26 T. J. Antosiewicz, S. P. Apell and T. Shegai, *ACS Photonics*, 2014, **1**, 454–463.
27 A. Cacciola, *et al.*, *ACS Nano*, 2014, **8**, 11483–11492.
28 T. Ambjörnsson, G. Mukhopadhyay, S. P. Apell and M. Käll, *Phys. Rev. B: Condens. Matter Mater. Phys.*, 2006, **73**, 085412.
29 R. Chikkaraddy, *et al.*, *Nature*, 2016, **535**, 127–130.
30 G. Zengin, T. Gschneidtner, R. Verre, L. Shao, T. J. Antosiewicz, K. Moth-Poulsen, M. Käll and T. Shegai, *J. Phys. Chem. C*, 2016, **120**, 20588–20596.
31 E. C. Le Ru, S. A. Meyer, C. Artur, P. G. Etchegoin, J. Grand, P. Lang and F. Maurel, *Chem. Commun.*, 2011, **47**, 3903.
32 C. Li, S. Lee, Z. Qian, C. Woods, S.-J. Park and Z. Fakhraai, *J. Phys. Chem. C*, 2018, **122**, 6808–6817.
33 M. R. Foreman and F. Vollmer, *Phys. Rev. Lett.*, 2015, **114**, 118001.
34 P. Törmä and W. L. Barnes, *Rep. Prog. Phys.*, 2015, **78**, 013901.
35 P. Fauché, S. G. Kosionis and P. Lalanne, *Phys. Rev. B*, 2017, **95**, 195418.
36 L. Zhao, T. Ming, L. Shao, H. Chen and J. Wang, *J. Phys. Chem. C*, 2012, **116**, 8287–8296.
37 S. Bidault, A. Devilez, P. Ghenuche, B. Stout, N. Bonod and J. Wenger, *ACS Photonics*, 2016, **3**, 895–903.
38 S. Sanders and A. Manjavacas, *ACS Photonics*, 2018, **5**, 2437–2445.
39 H. DeVoe, *J. Chem. Phys.*, 1964, **41**, 393.
40 V. A. Markel, L. S. Muratov, M. I. Stockman and T. F. George, *Phys. Rev. B: Condens. Matter Mater. Phys.*, 1991, **43**, 8183–8195.
41 V. A. Markel, MarCoDES: Markel's Coupled Dipole Equation Solvers, in *New Mexico state university user guide*, Department of Physics, 1998.
42 E. M. Purcell and C. R. Pennypacker, *Astrophys. J.*, 1973, **186**, 705–714.
43 M. Yurkin and A. Hoekstra, *J. Quant. Spectrosc. Radiat. Transfer*, 2007, **106**, 558–589.
44 D. J. Masiello and G. C. Schatz, *J. Chem. Phys.*, 2010, **132**, 064102.
45 H. Chew, *J. Chem. Phys.*, 1987, **87**, 1355–1360.
46 L. Novotny and B. Hecht, *Principles of Nano-Optics*, Cambridge University Press, Cambridge, 2006.
47 E. C. Le Ru and P. G. Etchegoin, *MRS Bull.*, 2013, **38**, 631–640.
48 F. W. King, R. P. V. Duyne and G. C. Schatz, *J. Chem. Phys.*, 1978, **69**, 4472–4481.
49 S. Efrima and H. Metiu, *J. Chem. Phys.*, 1979, **70**, 1602–1613.
50 W. H. Weber and G. W. Ford, *Phys. Rev. Lett.*, 1980, **44**, 1774–1777.
51 S. M. Barnett, N. Harris and J. J. Baumberg, *Phys. Chem. Chem. Phys.*, 2014, **16**, 6544–6549.
52 C. M. Teodorescu, *Phys. Chem. Chem. Phys.*, 2015, **17**, 21302–21314.
53 P. Bharadwaj and L. Novotny, *Opt. Express*, 2007, **15**, 14266–14274.
54 J. D. Jackson, *Classical electrodynamics*, Wiley, New York, 2nd edn, 1998.
55 M. Kasha, H. R. Rawls and E.-B. M. Ashraf, *Pure Appl. Chem.*, 2009, **11**, 371–392.
56 B. Auguié, J. L. Alonso-Gómez, A. Guerrero-Martínez and L. M. Liz-Marzán, *J. Phys. Chem. Lett.*, 2011, **2**, 846–851.
57 X. Yin, M. Schäferling, B. Metzger and H. Giessen, *Nano Lett.*, 2013, **13**, 6238–6243.
58 M. Born, *Phys. Z.*, 1915, **16**, 251–258.
59 W. Kuhn, *Z. Phys. Chem.*, 1929, **4**, 14–36.
60 H. DeVoe, *J. Chem. Phys.*, 1965, **43**, 3199–3208.
61 Z. Fan and A. O. Govorov, *Nano Lett.*, 2010, **10**, 2580–2587.

62 A. Guerrero-Martínez, J. L. Alonso-Gómez, B. Auguié, M. M. Cid and L. M. Liz-Marzán, *Nano Today*, 2011, **6**, 381–400.
63 A. O. Govorov, Z. Fan, P. Hernandez, J. M. Slocik and R. R. Naik, *Nano Lett.*, 2010, **10**, 1374–1382.
64 L. M. Kneer, E.-M. Roller, L. V. Besteiro, R. Schreiber, A. O. Govorov and T. Liedl, *ACS Nano*, 2018, **12**, 9110–9115.
65 B. L. Darby and E. C. Le Ru, *J. Am. Chem. Soc.*, 2014, **136**, 10965–10973.
66 H. K. Turley, Z. Hu, L. Jensen and J. P. Camden, *J. Phys. Chem. Lett.*, 2017, **8**, 1819–1823.
67 J. Zhao, L. Jensen, J. Sung, S. Zou, G. C. Schatz and R. P. Van Duyne, *J. Am. Chem. Soc.*, 2007, **129**, 7647–7656.

Electronic Supplementary Material (ESI) for Nanoscale.

Supporting Information for: Electromagnetic Interactions of Dye Molecules Surrounding a Nanosphere

Baptiste Auguié,*,†,‡,¶ Brendan L. Darby,† and Eric C. Le Ru†,‡

†*School of Chemical and Physical Sciences, Victoria University of Wellington, PO Box 600, Wellington, New Zealand*

‡*The MacDiarmid Institute for Advanced Materials and Nanotechnology*

¶*The Dodd-Walls Centre for Quantum and Photonic Technologies*

E-mail: baptiste.auguie@vuw.ac.nz

Contents

S1 Overview of the colloid and dye spectra

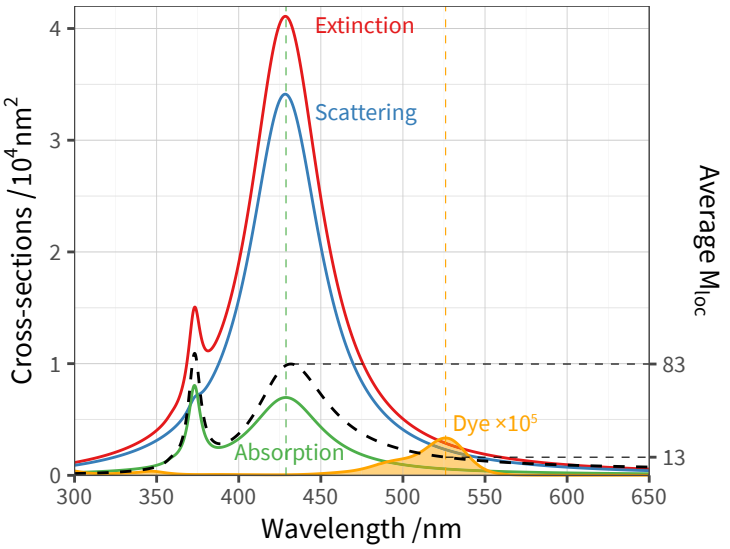

Figure S1: Simulated spectra of a 30 nm radius silver sphere in water, compared to the experimentally-derived absorption cross-section of the dye Rhodamine 6G (orange line, scaled up by a factor 10^5). The solid lines represent extinction (red), absorption (green) and scattering (blue) cross-sections. The dashed black line, with corresponding scale on the right side of the plot, presents the surface-averaged local-field intensity enhancement factor $\langle M_{\text{loc}} \rangle$.[1] The dye absorbance peaking at 526 nm is well-detuned from the plasmon resonances, and the enhancement factor is around 13 at that wavelength.

We reproduce for completeness in Fig. S1 the simulated optical response of a 30 nm radius silver sphere in water calculated with Mie theory[1,2] (far-field absorption, scattering, and extinction cross-sections (left scale), and surface-averaged local-field intensity enhancement factor M_{loc} (right scale)). For comparison, the spectrum of a single Rhodamine 6G dye is displayed, with a scaling factor of 10^5. Note the large detuning between the dye absorption maximum (526 nm) and the plasmon resonance (around 429 nm for the dipole resonance). Most figures in the manuscript focus on the changes in the dye's spectrum due to dipole-dipole and dipole-sphere electromagnetic interactions, rather than the plasmon resonances.

S2 Coupled dipole equations

We summarise below the standard equations of coupled-dipole theory in the more general case where the embedding medium is not necessarily vacuum/air, as no single convention exists for the various prefactors affecting the definition of polarisability and other quantities.

We consider a collection of N point electric dipoles $\mathbf{p}_i$ located at $\mathbf{r}_i$ and embedded in a homogeneous infinite medium characterised by a dielectric function ε_1. The dipoles are subject to an incident macroscopic field $\mathbf{E}^{\text{INC}}$. The response of the point dipoles $\mathbf{p}_i$ is assumed local and linear and described by a polarisability tensor (possibly different for each molecule)

as:

$$\mathbf{p}_i = \bar{\bar{\alpha}}_i \mathbf{E}_i, \tag{S1}$$

where $\mathbf{E}_i$ denotes the *macroscopic* field at the dipole position.

At a microscopic level, a dipole reacts to the applied field with an intrinsic polarisability $\bar{\bar{\alpha}}^{\mu}$. The applied field is enhanced by a local-field correction L arising from the polarisation of the embedding medium (Eq. S33 below). In turn, such a dipole moment produces a field which is enhanced by the same local field factor, from a reciprocity argument. We may therefore deduce the effective macroscopic polarisability $\bar{\bar{\alpha}}$ as

$$\bar{\bar{\alpha}} = L^2 \bar{\bar{\alpha}}^{\mu}. \tag{S2}$$

The macroscopic electric field created by such a dipole $\mathbf{p}_i$ at a general point $\mathbf{r}$ also depends linearly on that dipole moment,

$$\mathbf{E}_{\mathbf{p}_i}(\mathbf{r}) = \bar{\bar{G}}(\mathbf{r}_i, \mathbf{r})\, \mathbf{p}_i, \tag{S3}$$

where the Green's tensor $\bar{\bar{G}}$ characterises the electric field at $\mathbf{r}$ created by a unit point dipole at $\mathbf{r}_i$.

A given dipole responds to a net macroscopic field that is the sum of the incident field and the field scattered by its neighbours. With the above conventions, the coupled dipole equations take the form,

$$\mathbf{p}^i = \bar{\bar{\alpha}}_i \left(\mathbf{E}^{\text{INC}}(\mathbf{r}_i) + \sum_{j \neq i} \bar{\bar{G}}_{ij} \mathbf{p}^j \right), \tag{S4}$$

where $\mathbf{E}^{\text{INC}}(\mathbf{r}_i)$ is the incident field, and $\bar{\bar{G}}_{ij} = \bar{\bar{G}}(\mathbf{r}_i, \mathbf{r}_j)$ is the Green's tensor for the field created by dipole j at the location of dipole i in the infinite surrounding medium,

$$\bar{\bar{G}}_{ij} = \beta^{-1} \frac{e_{ij}^{ik_1 r}}{r_{ij}} \left\{ k_1^2 \left[\bar{\bar{I}} - \hat{\mathbf{r}}_{ij} \otimes \hat{\mathbf{r}}_{ij} \right] - \left(\frac{1}{r_{ij}^2} - \frac{ik_1}{r_{ij}} \right) \left[\bar{\bar{I}} - 3\hat{\mathbf{r}}_{ij} \otimes \hat{\mathbf{r}}_{ij} \right] \right\} \tag{S5}$$

k_1 is the wave vector in the embedding medium, and we introduced the prefactor $\beta = 4\pi\varepsilon_0\varepsilon_1$ which may be simplified throughout in practice by defining suitably-normalised quantities.

The absorption cross-section is given by:

$$\sigma_{\text{abs}} = \frac{4\pi\beta^{-1}k_1}{|E_0|^2} \sum_i \left(\Im \left[\mathbf{p}_i \cdot \mathbf{E}_i^* \right] - \frac{2\beta}{3} k_1^3 |\mathbf{p}_i|^2 \right). \tag{S6}$$

S3 Generalised Coupled Dipole Method (GCDM)

We now describe the additional terms introduced in the generalised coupled-dipole system (Eq. 2 of the main manuscript) by the introduction of the sphere, as well as the calculation of far-field cross-sections for the combined system in the framework of generalised Mie theory.

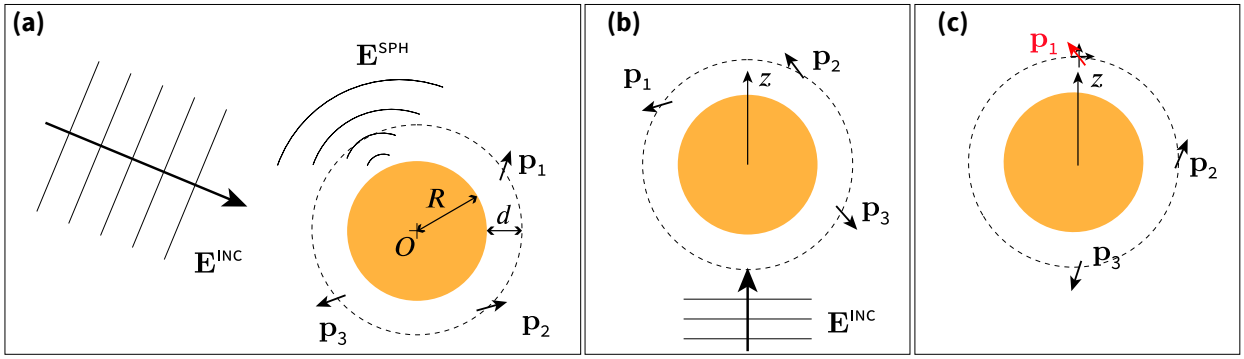

Figure S2: Schematic representation of the light scattering problem under study. (a) An incident plane wave with associated electric field $\mathbf{E}^{\mathrm{INC}}$ impinges on a spherical nanoparticle of radius R surrounded by polarisable dipoles in arbitrary positions and orientations at a distance d above the sphere. Each dipole responds to a net exciting field that comprises the incident plane wave, the scattered field from the sphere $\mathbf{E}^{\mathrm{SPH}}$, and the scattered field from all neighbouring dipoles in the presence of the sphere. (b) For convenience, in numerical calculations, the response of the dipoles to a plane wave is modelled by rotating the coordinates such that the incident wave propagates with wave vector along the z axis. (c) Similarly, the coupling between two dipoles is treated by considering the source dipole placed along the z axis, with appropriate rotations, and its decomposition along two orthogonal unit dipoles (normal and tangential to the sphere).

S3.1 Exciting field due to the sphere.

The net incident field on the collection of dipoles (source term in the linear system of Eq. 2) is augmented by the contribution $\mathbf{E}^{\mathrm{SPH}}$. For a given external incident field, such as a plane wave propagating along an arbitrary direction, we use the Mie theory[3] to compute the electric field scattered by the bare sphere at any point in space, and in particular at the location of each dipole. In practice, the calculation simplifies considerably and is therefore much more efficient when the plane wave is incident along the z axis (Fig. S2b). Our strategy is therefore to compute the electric field for a plane wave incident along the z axis on a fine grid of locations around the sphere and interpolate the (complex) vector components of this electric field distribution at the location of the dipoles in a suitably-rotated coordinate system for each required direction of incidence and polarisation.

S3.2 Coupling mediated by the sphere.

The Green tensor's contribution $\bar{\bar{S}}_{ij}$ expresses the field created at location $\mathbf{r}_j$ by a unit dipole at $\mathbf{r}_i$ due to scattering by the sphere. We calculate this 3×3 matrix using a generalised Mie theory, where the field of the exciting dipole $\mathbf{p}_i$ is decomposed in a basis of vector spherical

wavefunctions (VSWFs) centred on the sphere,[1,4,5]

$$\mathbf{E}^{\mathrm{i,DIP}} = \sum_{n=1}^{\infty}\sum_{m=-n}^{n} a_{mn}^{\mathrm{i,DIP}}\mathbf{M}^{(1)}(k_1,\mathbf{r}) + b_{mn}^{\mathrm{i,DIP}}\mathbf{N}^{(1)}(k_1,\mathbf{r}), \qquad r \le r_i, \tag{S7}$$

$$\mathbf{E}^{\mathrm{i,DIP}} = \sum_{n=1}^{\infty}\sum_{m=-n}^{n} e_{mn}^{\mathrm{i,DIP}}\mathbf{M}^{(3)}(k_1,\mathbf{r}) + f_{mn}^{\mathrm{i,DIP}}\mathbf{N}^{(3)}(k_1,\mathbf{r}), \qquad r \ge r_i. \tag{S8}$$

$(\mathbf{N}^{(3)},\mathbf{M}^{(3)}), (\mathbf{N}^{(1)},\mathbf{M}^{(1)})$ are the regular and irregular VSWFs, respectively, $a_{mn}^{\mathrm{i,DIP}}$, $b_{mn}^{\mathrm{i,DIP}}$, $e_{mn}^{\mathrm{i,DIP}}$, $f_{mn}^{\mathrm{i,DIP}}$ are expansion coefficients with known analytical expressions in terms of $\mathbf{p}_i$ (given in Sec. S2). The second expansion in terms of irregular waves will be used in the calculation of cross-sections.

The field scattered by the sphere from this dipolar excitation follows from Mie theory,

$$\mathbf{E}^{\mathrm{SCA}} = \sum_{n=1}^{\infty}\sum_{m=-n}^{n} p_{mn}\mathbf{M}^{(3)}(k_1,\mathbf{r}) + q_{mn}\mathbf{N}^{(3)}(k_1,\mathbf{r}) \tag{S9}$$

with

$$p_{mn}^{\mathrm{i,DIP}} = \Gamma_n a_{mn}^{\mathrm{i,DIP}}, \tag{S10}$$

$$q_{mn}^{\mathrm{i,DIP}} = \Delta_n b_{mn}^{\mathrm{i,DIP}}, \tag{S11}$$

where Γ_n and Δ_n are the standard electric and magnetic multipolar Mie susceptibilities.[1,3] Calculating this field for each dipole at all the other dipole positions can become too computationally intensive and impractical for a large number of coupled dipoles. We therefore again adopt an interpolation scheme to speed up this step: as with the case of plane wave illumination, the VSWF series simplify greatly if the source dipole is placed along the z-axis; we therefore evaluate the scattered field around the sphere for two independent unit dipoles placed along the z axis, and oriented radially or tangentially, respectively (Fig. S2c). For each dipole, we then perform the required rotations to bring it along the z axis and interpolate the field components at the location of the other dipoles, before rotating them back to the common reference frame.

S3.3 Far-field cross-sections.

A similar formal expansion to Eq. S7 is used for the plane wave illumination at arbitrary incidence (with different, known coefficients[5]) corresponding to the incident field,

$$\mathbf{E}^{\mathrm{INC}} = \sum_{n=1}^{\infty}\sum_{m=-n}^{n} a_{mn}^{\mathrm{PW}}\mathbf{M}^{(1)}(k_1,\mathbf{r}) + b_{mn}^{\mathrm{PW}}\mathbf{N}^{(1)}(k_1,\mathbf{r}). \tag{S12}$$

The sum of both incident and dipole fields forms the net exciting field for the sphere,

$$\begin{aligned}\mathbf{E}^{\mathrm{EXC}} &= \mathbf{E}^{\mathrm{DIP}} + \mathbf{E}^{\mathrm{INC}} \\ &= \sum_{n=1}^{\infty}\sum_{m=-n}^{n} a_{mn}^{\mathrm{EXC}}\mathbf{M}^{(1)}(k_1,\mathbf{r}) + b_{mn}^{\mathrm{EXC}}\mathbf{N}^{(1)}(k_1,\mathbf{r})\end{aligned} \tag{S13}$$

where we simply sum all dipole coefficients to those of the incident plane wave,

$$\begin{aligned}a_{mn}^{\mathrm{EXC}} &= a_{mn}^{\mathrm{PW}} + \sum_i a_{mn}^{\mathrm{i,DIP}}, \quad \text{and} \\ b_{mn}^{\mathrm{EXC}} &= b_{mn}^{\mathrm{PW}} + \sum_i b_{mn}^{\mathrm{i,DIP}}.\end{aligned} \tag{S14}$$

The coefficients for the field scattered by the sphere from the combined excitation follow from Mie theory,

$$p_{mn} = \Gamma_n a_{mn}^{\mathrm{EXC}}, \tag{S15}$$

$$q_{mn} = \Delta_n b_{mn}^{\mathrm{EXC}}. \tag{S16}$$

The total scattering cross-section is obtained by summing the total field scattered by the sphere, and that directly radiated by the dipoles (Eq. S8), both expressed in a basis of irregular VSWFs.

$$\sigma_{\mathrm{sca}} = \frac{1}{k_1^2}\sum_{n=1}^{\infty}\sum_{m=-n}^{n} |e_{mn}^{\mathrm{DIP}} + p_{mn}^{\mathrm{SPH}}|^2 + |f_{mn}^{\mathrm{DIP}} + q_{mn}^{\mathrm{SPH}}|^2 \tag{S17}$$

For the extinction cross-section we invoke the optical theorem, where the incident field is a plane wave excitation along a specific direction, and the scattered field is given by the superposition of the dipole sources and the total field scattered by the sphere, which results in:

$$\sigma_{\mathrm{ext}} = \frac{-1}{k_1^2}\sum_{n=1}^{\infty}\sum_{m=-n}^{n} \Re\left(a_{mn}^{\mathrm{PW}} p_{mn}^{*} + a_{mn}^{\mathrm{PW}} e_{mn}^{*\mathrm{DIP}}\right) + \Re\left(b_{mn}^{\mathrm{PW}} q_{mn}^{*} + b_{mn}^{\mathrm{PW}} f_{mn}^{*\mathrm{DIP}}\right). \tag{S18}$$

The absorption cross-section is then deduced as

$$\sigma_{\mathrm{abs}} = \sigma_{\mathrm{ext}} - \sigma_{\mathrm{sca}}. \tag{S19}$$

S3.4 Numerical implementation

We summarise our approach as follows:

- obtain the self-consistent macroscopic fields $\mathbf{E}_i$ and dipole moments $\mathbf{p}_i$ via the extended coupled-dipole system (Eq. 2)
- for each dipole $\mathbf{p}_i$, now considered as a source, calculate its expansion coefficients a_{nm}^i, b_{nm}^i, e_{nm}^i, f_{nm}^i

- define the total exciting field as the sum of expansion coefficients from all dipoles (Eq. S14), added to those corresponding to the incident plane wave
- multiply these incident field coefficients by the Mie susceptibilities Δ_n and Γ_n to obtain the scattered field coefficients (p_{nm}, q_{nm}) in response to this composite exciting field
- the optical cross-sections follow from these coefficients using Eqs. S17–S19.

In a practical numerical implementation, all the infinite series expansions must be truncated. We chose to truncate them at a maximum multipolar order $n_{\max}$ and include all $|m| \leq n$. The value of $n_{\max}$ was chosen such that the resulting cross-sections have converged to a good accuracy, i.e. do not vary with higher $n_{\max}$. We note that, although the Mie theory provides a rigorous analytical solution to the scattering problem, in practice the computation of the series can be problematic, as a large number of terms needs to be included for dipoles very close to the surface of the sphere (as many as $n_{\max} = 1000$ multipoles).[1,6,7] In order to alleviate the numerical difficulties in computing the Mie coefficients at very large order (which results in overflow when computing spherical Bessel functions), we use a fast-convergent electrostatic approximation[7] for terms above $n = 50$, and combine this solution to the exact Mie coefficients for $n < 50$. This is justified because the spherical Bessel functions $z_n(x)$ can be well approximated by their small-argument ($x \to 0$) approximation for $x \lesssim n$. Our tests indicate that this approximation yields results that have a relative accuracy better than 10^{-3}. A truncation value of $n_{\max} = 500$ was sufficient to reach results of comparable accuracy in all the calculations presented here.

S3.5 Expansion coefficients for plane wave and dipole

Our definitions for the vector spherical wavefunctions follow Mishchenko et al.;[5] we summarise below for convenience the expansion coefficients for a plane wave illumination[5] and a dipole source,[1] with reference to the equation number in the original source,

$$a_{mn}^{\mathrm{PW}} = 4\pi(-1)^m i^n r_n e^{-im\varphi} \hat{\mathbf{e}} \cdot \mathbf{C}_{mn}^*(\theta) \qquad \text{[C.57] in Ref. 5} \tag{S20}$$

$$b_{mn}^{\mathrm{PW}} = 4\pi(-1)^m i^{n-1} r_n e^{-im\varphi} \hat{\mathbf{e}} \cdot \mathbf{D}_{mn}^*(\theta) \tag{S21}$$

$$a_{mn}^{\mathrm{DIP}} = E_{p0}(-1)^m \hat{\mathbf{p}} \cdot \mathbf{M}_{-mn}^{(3)}(r,\theta,\phi) \qquad \text{[H.84] in Ref. 1} \tag{S22}$$

$$b_{mn}^{\mathrm{DIP}} = E_{p0}(-1)^m \hat{\mathbf{p}} \cdot \mathbf{N}_{-mn}^{(3)}(r,\theta,\phi) \tag{S23}$$

$$e_{mn}^{\mathrm{DIP}} = E_{p0}(-1)^m \hat{\mathbf{p}} \cdot \mathbf{M}_{-mn}^{(1)}(r,\theta,\phi) \qquad \text{[H.86] in Ref. 1} \tag{S24}$$

$$f_{mn}^{\mathrm{DIP}} = E_{p0}(-1)^m \hat{\mathbf{p}} \cdot \mathbf{N}_{-mn}^{(1)}(r,\theta,\phi) \tag{S25}$$

where we defined

$$r_n = \sqrt{\frac{2n+1}{4\pi n(n+1)}}, \tag{S26}$$

and $\hat{\mathbf{p}}$ and $\hat{\mathbf{e}}$ are unit vectors in the direction of $\mathbf{p}$ and $\mathbf{E}$, respectively. The prefactors for both fields are

$$E_0 = 1, \quad \text{(we assume a unit incident field throughout)} \tag{S27}$$

$$E_{p0} = \frac{ik_1^3 p}{\varepsilon_0 \varepsilon_1} = 4\pi i k_1^3 \beta^{-1} p, \qquad \text{[H.83] in Ref. 1} \tag{S28}$$

S4 Model dye polarisability

The model dye polarisability is the same as the one used in our previous study of dye interacting in the absence of the nanosphere. We recall it here for completeness.[8]

The polarisability tensors considered in the main manuscript for coupled-dipole simulations are either isotropic,

$$\bar{\bar{\alpha}} = \begin{pmatrix} \alpha_d & 0 & 0 \\ 0 & \alpha_d & 0 \\ 0 & 0 & \alpha_d \end{pmatrix}, \tag{S29}$$

or uniaxial,

$$\bar{\bar{\alpha}} = \begin{pmatrix} 0 & 0 & 0 \\ 0 & 0 & 0 \\ 0 & 0 & 3\alpha_d \end{pmatrix}. \tag{S30}$$

These tensors are expressed in their natural frame (where they are diagonal), and need to be rotated depending on molecular orientations. The factor of 3 in the second case ensures that the trace remains the same and that the orientation-averaged absorption is the same in both cases.

We take the following model (single Lorentzian) to describe the microscopic polarisability of a dye in a vacuum,

$$\alpha_d = \alpha_\infty + \frac{\alpha_1 \lambda_1}{\mu_1} \left[\frac{1}{1 - \frac{\lambda_1^2}{\lambda^2} - i\frac{\lambda_1^2}{\lambda \mu_1}} - 1 \right] \tag{S31}$$

For a simplified model of a dye resembling Rhodamine 6G, we use $\alpha_\infty = 3.2 \times 10^{-39}\,[\mathrm{SI}]$, $\alpha_1 = 1.92 \times 10^{-38}\,[\mathrm{SI}]$, $\lambda_1 = 526\,\mathrm{nm}$, $\mu_1 = 10^4\,\mathrm{nm}$. We emphasise that for the concentration-dependence to be meaningful the magnitude of α_d must be correct. In many studies, this is freely adjusted to match experimentally-observed spectral shifts. Here, we instead use the experimentally measured absorption cross-section to determine the absolute α_d, as discussed in Ref. 9. Taking into account the local-field enhancement of the solvent (of refractive index $n = \sqrt{\varepsilon_1}$), the absorption cross-section of an isolated dye in water is given by[1,9]

$$\sigma_{\mathrm{abs}}(\lambda) = \frac{2\pi}{\lambda \varepsilon_0 \sqrt{\varepsilon_1}} L^2 \mathrm{Im}\left(\alpha_d(\lambda)\right) \tag{S32}$$

with the local field factor

$$L = \frac{\varepsilon_1 + 2}{3}. \tag{S33}$$

S5 Self-reflected field in the electrostatic-planar approximation

The self-reflected field is given by the field created by the dipole image,[1,10]

$$\mathbf{E}^{\text{SR}} = \left(\frac{\varepsilon_2 - \varepsilon_1}{\varepsilon_2 + \varepsilon_1}\right) \frac{2\mathbf{p}_\perp + \mathbf{p}_\parallel}{4\pi\varepsilon_0\varepsilon_1(2d)^3}, \tag{S34}$$

where $\mathbf{p}_\perp$ and $\mathbf{p}_\parallel$ are the components of the dipole normal or tangential to the metal surface. This is equivalent to the approximation:

$$\bar{\bar{S}}_{11} \approx \left(\frac{\varepsilon_2 - \varepsilon_1}{\varepsilon_2 + \varepsilon_1}\right) \frac{1}{4\pi\varepsilon_0\varepsilon_1(2d)^3} \left(\begin{smallmatrix} 1 & 0 & 0 \\ 0 & 1 & 0 \\ 0 & 0 & 2 \end{smallmatrix}\right). \tag{S35}$$

For a general external field $\mathbf{E}^{\text{EXT}}$, the induced dipole is $\mathbf{p}_1 = \bar{\bar{\alpha}}_1(\mathbf{E}^{\text{EXT}} + \mathbf{E}^{\text{SR}})$, and we may describe the net response in terms of an effective polarisability: $\mathbf{p}_1 = \bar{\bar{\alpha}}_{\text{eff}}\mathbf{E}^{\text{EXT}}$, with

$$\bar{\bar{\alpha}}_{\text{eff}} = (\bar{\bar{I}} - \bar{\bar{\alpha}}_1\bar{\bar{S}}_{11})^{-1}\bar{\bar{\alpha}}_1. \tag{S36}$$

Substituting Eq. S35 into Eq. S36, we can predict the modified absorbance of a single dipole (proportional to $\Im(\alpha_{\text{eff}})$) in the electrostatic-planar approximation.

S6 Effect of the dye orientation and coverage uniformity

In Fig. 7 of the main manuscript we present a comparison with experimental data for a chosen configuration with uniaxial dyes oriented at $\theta = 75°$ from the normal to the surface, and a random coverage of the sphere surface. We provide in Fig. S3 further simulations to explore the influence of both parameters. The non-uniform coverage of the surface broadens the spectral features, and shows an onset of spectral shifts at a lower concentration than with a more uniform coverage; this is expected because randomly-chosen positions yield a broader range of pair-wise distances between nearest neighbours, and in particular shorter distances responsible for the more prominent spectral shifts. The molecule's orientation with respect to the surface normal is an important parameter for the simulations; it affects the intensity of the local field, and therefore the differential absorbance (compare the scale of panels (a) and (e)), but also the spectral shifts through dye-dye interactions. Comparing the predicted absorbance spectra to those observed experimentally suggests that an adsorption geometry of around 75° yields the closest agreement.

References

(1) Le Ru, E. C.; Etchegoin, P. G. *Principles of Surface Enhanced Raman Spectroscopy and Related Plasmonic Effects*; Elsevier: Amsterdam, 2009.

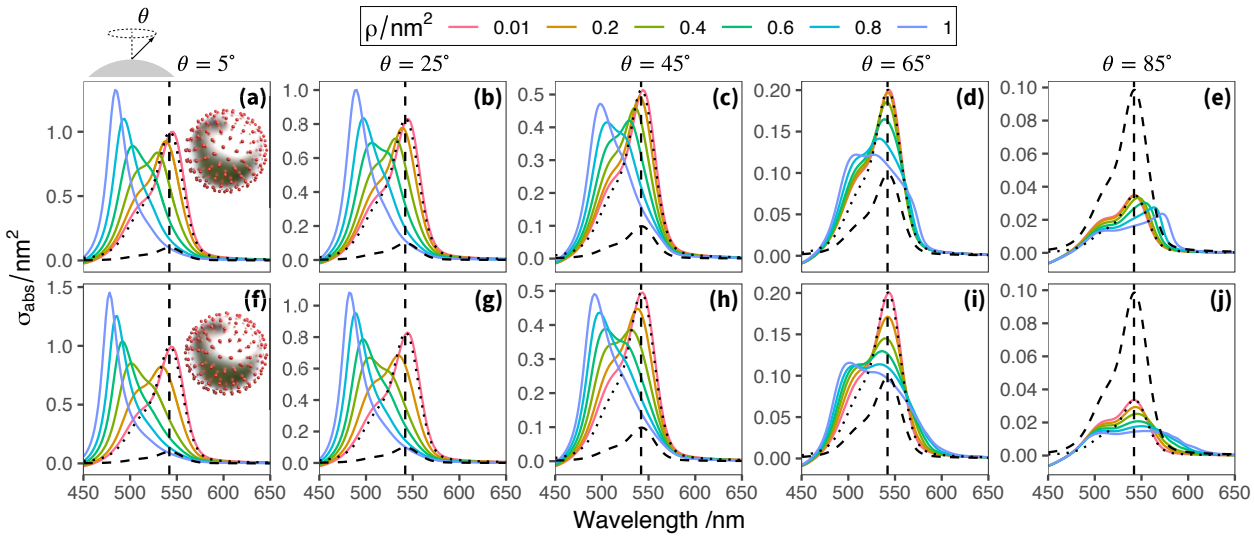

Figure S3: Differential absorbance spectra for uniaxial dipoles titled by an angle θ from the surface normal with either uniform coverage (Top row a–e) or random positions on the sphere with a minimal exclusion distance of 0.7 nm between any two neighbours (Bottom row f–j). We vary the tilt angle from 5° to 85°, and the surface concentration ρ. The dashed line, common to all panels, is the absorption of the isolated dye in the embedding medium without the sphere. For ease of comparison of the spectral shape, the dotted line presents the same data rescaled to the maximum of the low-concentration predictions with the sphere.

(2) Le Ru, E. C.; Etchegoin, P. G. SERS and Plasmonics Codes (SPlaC). Matlab codes freely available from http://www.vuw.ac.nz/raman/book/codes.aspx, 2009.

(3) Bohren, C. F.; Huffman, D. R. *Absorption and scattering of light by small particles*; Wiley-VCH: Weinheim, 2004; OCLC: 254937169.

(4) Chew, H. Transition rates of atoms near spherical surfaces. *J. Chem. Phys.* **1987**, *87*, 1355–1360.

(5) Mishchenko, M. I.; Travis, L. D.; Lacis, A. A. *Scattering, absorption, and emission of light by small particles*; Cambridge University Press, 2002.

(6) Moroz, A. Superconvergent Representation of the Gersten–Nitzan and Ford–Weber Nonradiative Rates. *J. Phys. Chem. C* **2011**, *115*, 19546–19556.

(7) Majić, M. R. A.; Auguié, B.; Le Ru, E. C. Spheroidal harmonic expansions for the solution of Laplace's equation for a point source near a sphere. *Phys. Rev. E* **2017**, *95*, 033307.

(8) Auguié, B.; Le Ru, E. C. Optical Absorption of Dye Molecules in a Spherical Shell Geometry. *J. Phys. Chem. C* **2018**, *122*, 19110–19115.

(9) Djorović, A.; Meyer, M.; Darby, B. L.; Le Ru, E. C. Accurate Modeling of the Polarizability of Dyes for Electromagnetic Calculations. *ACS Omega* **2017**, *2*, 1804–1811.

(10) Bharadwaj, P.; Novotny, L. Spectral dependence of single molecule enhancement. *Opt. Express* **2007**, *15*, 14266–14274.